Understanding Severe Winter Haze Pollution in the North-Central North China Plain in 2014

Zhicong Yin[12], Huijun Wang[123], Huopo Chen[231]

[1]Collaborative Innovation Center on Forecast and Evaluation of Meteorological Disasters/Key Laboratory of Meteorological
5   Disaster, Nanjing University of Information Science & Technology, Nanjing, China
[2]Nansen-Zhu International Research Centre, Institute of Atmospheric Physics, Chinese Academy of Sciences, Beijing, China
[3]Climate Change Research Center, Chinese Academy of Sciences, Beijing, China

Correspondence to: Zhicong Yin (yinzhc@163.com)

Abstract. Atmospheric pollution has become a serious environmental and social problem in China. The winter
10   (December–February) haze days over the North-Central North China Plain (WHD_{NCP}) in 2014 was the highest in the past 30
years. Thus, it is necessary to analyze atmospheric pollution of this year in detail. Taking the anti-cyclone circulation over
North China as an intermediary, the positive phases of the East Atlantic/West Russia (EA/WR), the Western Pacific (WP) and
the Eurasia (EU) patterns led to a stable atmosphere that contributed to a larger number of WHD_{NCP}. In 2014, these three
patterns could be recognized from the wind anomalies in the lower troposphere, which can influence WHD_{NCP}. The
15   pre-autumn (September–November) Arctic sea ice (ASI) anomalies over the Eastern Hemisphere and the warmer winter
surface over Eurasia might have induced or intensified the positive EA/WR pattern in 2014. These two external forcings,
together with the pre-autumn sea surface temperature anomaly in the Pacific, might have also stimulated or enhanced the
positive EU-like patterns. The anomalous surface temperature in autumn 2014 was efficient in intensifying anomalous
circulations such as the positive phase of the WP pattern. The opposite case of minimum WHD_{NCP} in 2010 further supports the
20   mechanism of how EA/WA and WP patterns and associated external factors impact the WHD_{NCP}.

1.   Introduction

Related to booming economic development, atmospheric pollution has become a serious environmental and social problem
in China (Ding et al. 2014; Wang et al. 2016). Particularly after the persistent heavy fog and haze events in January 2013,

haze pollution has become more severe (Zhang et al. 2014; Zhao et al. 2014; Li et al. 2015) and has presented certain

25 negative effects on human health (Yin et al. 2011; Chen et al. 2013). The North-Central North China Plain (NCP), a location

in which the population density is quite high, was one of three haze-prone regions in China. The haze pollution over NCP

$(34\text{–}43^{o}\text{N}, 114\text{–}120^{o}\text{E})$ in 2013 and 2014 was the most serious of these events in the past 30 years (Yin et al. 2015a).

Therefore, the objective of this study was to examine the related atmospheric circulation anomalies and external forcings that

were responsible for the extreme haze pollution that occurred in winter (December–February) 2014.

30 In addition to pollutant emission, meteorological conditions are also vital contributors to haze occurrence (Liao et al. 2014;

Wang et al. 2016). Early studies documented that the East Asian winter monsoon (EAWM) had weakened after 1986, which

led to an increase of winter haze days (WHD) over NCP (WHD_{NCP}) (Yin et al. 2015a; Yin et al. 2015b; Li et al. 2015). The

decline of the preceding autumn (September–November) Arctic Sea Ice (ASI) from 1979 to 2012 greatly intensified haze

pollution in eastern China, the variance contribution of which was 45–67% (Wang et al. 2015a). Another external forcing,

35 sea surface temperature (SST) over the subtropical western Pacific (SWP), showed significantly negative correlation with

WHD_{NCP}. SWP-SST weakened EAWM circulation, leading to a favorable environment for haze with high static stability and

potential for hygroscopic growth (Yin et al. 2015c).

The obvious anti-cyclone anomaly around NCP was the most prominent circulation related to WHD_{NCP} (Yin et al. 2015c;

Chen et al. 2015) and was located near the bonding area of two continental Rossby waves, i.e., Eurasia (EU) and East

40 Atlantic/West Russia (EA/WR) patterns. The EU pattern, as defined by Wallace et al. (1981), originated from the

high-latitude polar region. The EU positive phase showed negative centers over the polar region $(70\text{–}80^{o}\text{N}, 60\text{–}90^{o}\text{E})$ and the

Japan Sea $(35\text{–}45^{o}\text{N}, 120\text{–}140^{o}\text{E})$, and a positive center over Mongolia and North China $(45\text{–}55^{o}\text{N}, 90\text{–}110^{o}\text{E})$, which

accounted for the severe drought in 2014 (Wang et al. 2015b). Another Eurasian teleconnection, known as the EA/WR

pattern (Barnston et al. 1987), was composed of negative centers over Central-North Atlantic and to the north of the Caspian

45 Sea, and positive centers over Europe and North China. The positive phase of these two continental Rossby wave trains

might have led to significant warming over the northern portion of Eastern Asia (Liu et al. 2014), indicating weaker cold air.

Therefore, we speculated that external forcings such as the SST, ASI and land surface temperature (TS) might impact

WHD$_{NCP}$ remotely by inducing teleconnection patterns in the atmosphere. Climate research on haze pollution in China is quite a new endeavor but is still insufficient, especially with respect to investigation into the mechanism that causes extreme

50   haze events. Thus, the impact of climate change on the persistent winter haze in 2014 over NCP is investigated in this study and is expected to improve prediction skill for WHD$_{NCP}$.

The remainder of this paper is organized as follows. The data and methods are clearly explained in Section 2. The climatic reality of severe WHD$_{NCP}$ in 2014 and associated atmospheric circulations are analyzed in Section 3. Section 4 describes investigation of the physical mechanism using the singular value decomposition (SVD) technique. Brief conclusions and

55   selected discussions are presented in Section 5.

2.   Datasets and methods

The China ground observations from 39 NCP stations (Figure 1) collected by the National Meteorological Information Center of China from 1979 to 2015 were used to reconstruct the climatic WHD data, referred to Yin et al. (2015c). After quality control, only four rural stations were selected, and the datasets tended to represent the characteristics of urban haze.

60   The weather measurements included relative humidity, visibility and wind speed that were collected four times per day, i.e., 02:00 local time (LT), 08:00 LT (00:00 UTC), 14:00 LT, and 20:00 LT. In this work, haze is recognized when visibility falls below a certain threshold and the relative humidity is less than 90%. After excluding other weather phenomena that affect visibility, a day with haze occurring at any time is defined as a haze day. Most of the visibility observations have switched from manual to automatic since Jan 1st, 2014, but the trial stations coded 54511, 54527 and 54623 were switched in 2013.

65   Thus, the visibility threshold is 10 km before Jan 1st, 2014 for most stations, but before Dec 1st, 2013 for the trial stations. After the switch, the threshold is 7.5 km, according to the China Meteorology Administration's notification (2014). To a certain extent, the WHD data of 2013 and 2014 are more qualitative than quantitative. To avoid continuity problems, the haze data for these two years were processed using composite analysis instead of correlation analysis in this study.

Haze is a multidisciplinary phenomenon that can be represented by visibility and humidity in meteorology and by the

70   concentration of the atmospheric composition in environmental science. In recent years, the atmospheric compositions

involving the concentrations of SO_2, NO, NO_2, NO_x, CO, O_3, $PM_{2.5}$ (by TEOM 1400a) and nephelometric turbidity (NEP) were measured in Shangdianzi and Baolian, an urban site (Zhao et al. 2011). The detailed atmospheric composition datasets were collected four times per day from Dec 1st, 2014 to Feb 28th, 2015. The hourly $PM_{2.5}$ data from 2004 to 2015 were observed at Shangdianzi Station, one of the six regional global atmospheric watch stations (GAWS) in China. Shangdianzi

75 Station is located at 40°39′N, 117°7′E and at a height of 293.3 m, which shelters it from human activities and pollution sources. As the only GAWS in North China, the atmospheric composition at this location was chosen to best reflect the natural state or rather the background conditions of the atmosphere (Yao et al. 2012). The $PM_{2.5}$ data were monitored every 5 minutes using two methods: tapered element oscillating microbalance (TEOM) and β-ray (since 2013).

In China, the temporal range and quality of the observed atmospheric compositions cannot support climatic haze research. To

80 demonstrate the representation of haze data reconstructed primarily by visibility, the hourly visibility and concentration of the atmospheric composition were shown, and the correlation coefficients were computed (Figure 2). In addition to significantly positive correlation with O_3, the correlation coefficients between visibility and seven compositions were all negative and exceeded the 99.99% confidence level in winter 2014. $PM_{2.5}$ was the main reason for haze pollution, and the correlation coefficients with visibility in Beijing were −0.51 (Baolian) and −0.48 (Shangdianzi). When visibility was less

85 than 7.5 km and 1 km, the mean $PM_{2.5}$ mass concentrations at Baolian were approximately greater than 100 and 200μg/m³, respectively. Thus, the tendency and magnitude both showed that the derived haze datasets not only agreed with the meteorological standard but also satisfactorily represented the concentration of the atmospheric composition.

Monthly atmospheric data such as wind, geopotential height, temperature and sea level pressure (SLP) are derived from the National Centers for Environmental Prediction/National Center for Atmospheric Research (NCEP/NCAR) global reanalysis

90 dataset with a horizontal resolution of 2.5°×2.5° collected from 1979 to 2015 (Kalnay et al. 1996). The monthly mean Extended Reconstructed SST (ERSST) datasets with a horizontal resolution of 2°×2° collected from 1979 to 2015 were obtained from the National Oceanic and Atmospheric Administration (NOAA) (Smith et al. 2008). The ASI extent was calculated using the ASI concentration data from Hadley Center's HadISST1 with a resolution of 1°×1° collected from 1979 to 2015 (Rayner et al. 2003). The EA/WR and WP indices were computed by the NOAA climate prediction center according

95   to the Rotated Principal Component Analysis (RPCA) used by Barnston et al. (1987). The calculation procedure for the EU

index was consistent with that of Wang et al. (2015b).

$$\text{EU index} = \left[-1 \times \overline{H500}_{(70-80^oN,60-90^oE)} + 2 \times \overline{H500}_{(45-55^oN,90-110^oE)} - 1 \times \overline{H500}_{(35-45^oN,120-140^oE)}\right]/4$$

where H500 represents the geopotential height at 500 hPa and overbars denote the area average.

To verify the covariability between the air and external forcings, i.e., SST, ASI and TS, SVD and correlation analyses were

applied after linear trends were removed. The anomalies in 2010, 2013 and 2014 were calculated relative to the climatic

100   mean of 1979-2012 without detrending. The site WHD data were converted into grids using the Cressman interpolation

(Cressman, 1959), and WHD_{NCP} was computed as the mean value of the grid data.

3.   Variations of WHD_{NCP} and associated atmospheric circulations

According to Figure 3, WHD_{NCP} from 1979 to 2012 can be divided into two decadal stages, i.e., the first stage from 1979 to

1992 with an average of 45.1 days and the second decade from 1993 to 2012 with an average of 34.5 days. It is obvious that

105   WHD_{NCP} exhibited rapid increase since winter 2010 with a large trend of 7.36 d/yr. NCP is a haze-prone area in which WHD

is distributed nonuniformly (Figure 4a). Two regions exhibited greater WHD: the plain to the east of Taihang Mountains and

to the south of Yan Mountains (PETSY) and the south of Shandong Province. Figure 4b shows the WHD anomaly in 2014

with respect to 1979–2012. In addition to a few sites, a larger number of WHD occurred, especially on the border of

Shandong and Henan and the northeast of Hebei. It is interesting to note that that WHDs in these two regions show

110   significant increases, filling up the climatic WHD valley as shown in Figure 4a. As a result, the haze-prone stations joined

together, indicating that the haze pollution was more serious in this region. At the same time, a larger number of WHD

occurred on PETSY and the south of Shandong Province. Recently, the haze pollution has become increasingly serious, as

shown by the number of haze days and its coverage. The percentages of sites with greater than 30 and 60 hazy days were

71.8% and 51.3%, respectively, in 2014. As shown in Figure 2, the mean $PM_{2.5}$ mass concentrations in Beijing were

115   approximately $100\mu g/m^3$ on hazy days, which indicates serious pollution in 2014. Although data continuity was influenced

by the switch of the observation method in 2013, the observation that WHD_{NCP} in 2014 was greater than before shows

robustness. Thus, it is reasonable to treat the year 2014 as a typical case for haze pollution over this region. As shown in Figure 3, NCP experienced the least WHD in 2010, which could be analyzed as an inverse case of the extreme haze phenomena.

120   In winter, the negative SLP anomaly in the Siberia region and the Chinese Mainland and the positive SLP anomaly over the West Pacific led to a reduced pressure gradient and weakened EAWM (Figure 5a). The weaker EAWM induced the southeasterly anomaly and reduced the surface wind speed (Figure 5c), indicating weaker cold air and a warmer land surface over NCP (Figure 5a). Influenced by the circulations with weaker cold air, horizontal diffusion of the atmospheric particulates was impeded, which was beneficial for haze occurrence. In the winter of 2014, the surface temperature of the

125   Asian continent was higher, illustrating that the EAWM was weaker from the source region to its south margin (Wang et al. 2015). The continental and oceanic SLP anomalies stimulated a significant southerly anomaly to the north of 50°N, blocking the cold air from high latitudes (Figure 5b). A southerly and smaller surface wind speed anomaly also occurred over the coastal area in the east of China (Figure 5d), resulting in more WHD$_{NCP}$.

In the mid-high layers of the troposphere, the correlation fields between WHD$_{NCP}$ and H500 (UV850) represented obvious

130   EA/WR and WP patterns (Figure 6a–b). The EA/WR pattern originated from the north-central Atlantic and propagated through Europe, the north of Caspian Sea and North China (Barnston et al. 1987; Liu et al. 2014). The WP pattern showed two activity centers, i.e., the broad area of Southeast Asia and the northwest Pacific and the Kamchatka Peninsula (Barnston et al. 1987). In addition to EA/WR, the EU pattern was another continental Rossby wave train over Eurasia, which significantly impacted the climate of East Asia. Although the EU pattern was unclear in Figure 6a–b, it can be recognized

135   distinctively from the anomalous circulations in 2014 (Figure 6c). The correlation coefficients between WHD$_{NCP}$ and these three pattern indices were calculated (Table 1). After detrending, WHD$_{NCP}$ showed significant positive correlation with both the EA/WR and WP patterns, indicating the remote impact on WHD$_{NCP}$ from land and sea. The correlation between EU and WHD$_{NCP}$ was initially significantly positive but became insignificant after detrending. Considering that EU could be recognized from low, middle and high layers in winter 2014, the EU pattern was still treated as a possible circulation

140   correlated with WHD$_{NCP}$. These patterns might contribute to WHD$_{NCP}$ by impacting the pivotal and local anti-cyclone

anomaly over NCP. The deep and broad positive anomaly confined the particles within a thinner boundary layer by suppressing vertical movement and progressed easterly to weaken the East Asia Jet Stream (EAJS), indicating weaker meridional cold air. In 2014, many extreme climatic events occurred, such as severe drought and high temperatures in NCP (Wang et al. 2015). Corresponding external forcings should be observed as the background of these extreme synoptic and climatic events, which might persistently impact the atmospheric circulations, leading to an irregular distribution of teleconnection patterns in winter. It should be noted that EA/WR pattern in winter 2014 was distributed slightly westwards and broadly. Nevertheless, the three eastern centers of EA/WR, WP and EU patterns could be recognized clearly (Figure 6c). Circulations such as the negative phase of EA/WR and WP were quite clear in 2010 (Figure 6d), leading to a favorable environment for diffusion with stronger cold air and vertical movement. This observation further supports the speculation that the anomalous EA/WR and WR patterns contribute to significant changes in WHD_{NCP}. The anomalies of the EU pattern in winter 2010 were not as significant as those in 2014. As shown by Table 1, the relationship between WHD_{NCP} and the EU index weakened after detrending, illustrating that the correlation was much weaker than the other two patterns.

4.   Possible mechanisms for the winter haze in 2014

In the above discussion, we addressed the associated circulations that were characterized by EA/WR, WP and EU patterns and that contributed to the extreme haze pollution in 2014. Wang et al. (2015a) found that the pre-autumn ASI could significantly impact the WHD in the east of China. As another efficient external forcing, the negative SWP-SST anomaly (SSTA) markedly intensified WHD_{NCP} (Yin et al. 2015c). Thus, the question arises as to whether these factors could have caused the extreme haze pollution that was measured in 2014.

Since 1979, the pre-autumn ASI declined substantially, which might impact the winter climate of East Asia (Liu et al. 2012). Furthermore, this decreasing trend of the ASI intensified from 2006 (Wang et al. 2015a), attracting global attention. The relationship between the pre-autumn ASI and the circulations was analyzed using the SVD method, explaining 51.6% and 17.9% of the variance by the first (SVD1) and second (SVD2) mode, respectively. The correlation coefficient of the first temporal series was 0.76, which was significantly above the 99% confidence level. The excited anti-cyclonic (A) or cyclonic

(C) activity centers of H500 in winter were located over the north Atlantic, Europe, to the north of Caspian Sea and around

165 Mongolia and North China, which appeared as the positive phase of the EA/WR pattern (Figure 7a). The corresponding

pre-autumn ASI, with more sea ice (SI) over the Barents Sea, Kara Sea and Laptev Sea (BKLSI) and less SI in the East

Siberian Sea (ESSI) could have contributed to the positive EA/WR pattern (Figure 7b). The anomalous ASI of the Eastern

Hemisphere in 2014 was similar to that shown in Figure 7b. According to the SVD results, the pre-autumn ASI anomalies in

2014 might have triggered the EA/WR pattern in the atmosphere and led to greater WHD_{NCP}. In autumn 2010, less BKLSI

170 and more ESSI (Figure S1) occurred, which might have induced less WHD over NCP.

In winter 2014, the TS anomalies of the broad region of Eurasia (40–70°N) was obviously positive. EA/WR is a famous

continental teleconnection, and a significant land-air interaction could influence the EA/WR pattern. To illustrate this

concept, an SVD analysis was performed between the detrended and normalized winter TS and H500 (Figure 8). The

explained variance (EV) and correlation coefficient of the first component were 53.3% and 0.73, respectively. The spatial

175 coefficients of TS were distributed similarly with TS anomalies in 2014. The associated circulations displayed three

anomalous centers, i.e., a positive center over Europe, negative anomalies to the north of Caspian Sea, and another positive

center over Mongolia and North China, which were also the three atmospherically active centers of EA/WR on the continent.

These results indicated that the TS anomalies of winter 2014 could have induced or intensified the positive EA/WR phase

and resulted in the extreme WHD_{NCP} case in 2014. In winter 2010, the cooler land surface of mid-latitude Eurasia (Figure S2)

180 could have contributed to the negative EA/WR phase. The diagnostic analyses of two inversely extreme WHD_{NCP} cases

enhanced the relationship between the winter mid-latitude Eurasia TS and WHD_{NCP}.

Figures 7 and 8 also show negative anomalies over the polar area (70–80°N, 60–90°E) and a positive center over Mongolia

and North China (45–55°N, 90–110°E), which can be recognized as a positive EU phase. When BKLSI was above normal

and ESSI was below normal or the surface of mid-latitude Eurasia was warmer, these two centers could be stimulated or

185 enhanced and represented favorable circulations for haze occurrence. Prior to this study, Yin et al. (2015c) found that the

pre-autumn SSTA of the Pacific excited atmospheric responses, including anti-cyclone anomalies over North China, and

resulted in more WHD_{NCP}. The SST in October and November (ON) and winter H500 were decomposed using the SVD

technique to reveal the main relationships. The EV and the correlation coefficient of the first component were 60.2% and

0.73, respectively. An EU-like pattern occurred in the first mode of H500, i.e., cyclonic anomalies over the polar area and

190   anti-cyclonic anomalies over Mongolia and North China (Figure 9a). The associated SST was cooler over the northwest

Pacific, involving Kuroshio and its extension, and warmer over the central-east Pacific and Alaska Gulf (Figure 9b). Another

atmospheric response was the weaker East Asia trough, indicating weaker EAWM and cold air. Figure 9c shows the ON

SSTA of the Pacific in 2014, which appeared to be similar to the SST SVD1 distribution and stimulated haze-prone

responses. In 2010, the ON SSTA in the Pacific did not show a well-organized opposite pattern (Figure S3), but a cooler SST

195   was observed on the central-east Pacific and Alaska Gulf, which were of benefit to haze occurrence.

Both EA/WR and EU were continental teleconnection patterns that propagated over Eurasia. In contrast, the WP pattern was

located over the junction of the marine and mainland areas, and its positive phases were composed of a broad positive center

over the northwest Pacific and Southeast Asia and a negative center over Kamchatka Peninsula (Barnston et al. 1987). From

Table 1, the stronger WP positive phase could have contributed to more WHD_{NCP} and could also have been partially

200   responsible for the severe haze event in 2014. To identify the causes of such circulations, we performed an SVD analysis

between winter H500 and pre-autumn TS, with EV values of 39.8% and 20.7%, respectively, for SVD1 and SVD2. The

results of SVD2 showed significant anomalies in the two centers of the positive WP pattern and anomalous TS distributed

from the southwest to the northeast in Eurasia (Figure 10). The correlation coefficient of the SVD2 time series was 0.62,

exceeding the 99% confidence level. Similar to the SVD2 representation, two "southwest to northeast" anomalous TS

205   distributions also occurred in autumn 2014, i.e., negative anomalies from the Caspian Sea to Baikal Lake and a positive

anomalous belt from Southwest China to Northeast China (Figure 10c). Referring to SVD2, these "southwest to northeast"

TS anomalies could have induced atmospheric responses over the junction of the Pacific and Asian land, which resembled

the WP pattern and impacted the local circulations over the NCP area. In autumn 2010, the positive belt of TS from the

Caspian Sea to Baikal Lake was significant, and the land surface of the Tibet Plateau was warmer than normal (Figure S4).

210   These two anomalies were dramatically inverted with the SVD2 results and could have stimulated a negative WP pattern. As

argued by two opposed cases, the mechanism for how the EA/WA and WP patterns and associated external factors impacted

the WHD$_{NCP}$ were confirmed.

5.   Conclusions and discussions

Except for a few sites, haze pollution over NCP in winter 2014 was the severest in the past 30 years. On the border of
Shandong and Henan and the northeast of Hebei, WHD increased significantly and filled up the climatic WHD valley,
illustrating a joint and broad severe haze-prone region. Taking the anti-cyclone anomalies over North China as an
intermediary, the positive phases of EA/WR, WP and EU patterns led to a stable atmosphere, which was beneficial for haze
occurrence. The anti-cyclone anomalies over East Asia not only resulted in stable atmospheric stratification and a thinner
boundary layer but also led to a southeasterly anomaly that weakened the cold air but enhanced the moisture transport. In
winter 2014, teleconnection patterns, such as EA/WR, EU and WP, combined to contribute to the extreme haze case. SVD
analyses indicated that the pre-autumn ASI anomalies of the Eastern Hemisphere and the warmer winter surface of Eurasia
could have induced or intensified the responses in the atmosphere, resembling a positive EA/WR pattern. These two external
forcings, together with the SSTA in Pacific (i.e., cooler in the northwest Pacific and warmer in the central-east Pacific and
Alaska Gulf) might stimulate or enhance positive EU-like patterns. In autumn 2014, the "southwest to northeast" anomalous
TS belts were other factors that efficiently intensified the haze pollutions, which resulted in a positive phase of the WP
pattern. The case of 2010, with the least WHD$_{NCP}$, was diagnosed as an opposite case, which further supports the speculation
that the anomalous EA/WR and WR patterns and associated external forcings have a significant impact on WHD$_{NCP}$.

The rapid increase of WHD$_{NCP}$ began in January 2013, and in winter 2013 and 2014, WHD$_{NCP}$ was significantly greater than
before. The WHD$_{NCP}$ in 2013 and 2014 was greater than 50 days and almost equal to each other (Figure 2). Therefore, the
causes of serious haze in 2013 should also be discussed. The anomalous circulations in winter 2013 were not as favorable for
haze conditions as those in 2014. The EA/WR pattern was well organized and showed a positive phase distributed slightly
eastwards (Figure S5). The EU and WP patterns were unclear. The source region of EU even showed characteristics of a
negative phase. From the perspective of anomalous circulation, the main cause contributing to serious WHD$_{NCP}$ in 2013 was
the remote impact of the EA/WR Rossby wave and appeared weaker than that in 2014. According to the 2010 and 2014 case

235   studies, the proceeding and simultaneous external forcings could have impacted the WHD$_{NCP}$. In contrast, the pre-autumn ASI and TS and winter TS in 2013 did not show features similar to those in 2014 (Figure S6). The pre-autumn Pacific SSTA, which was slightly negative in the northwest Pacific and positive in the Alaska Gulf and central-east Pacific, could have stimulated positive anomalies over NCP and weakened the East Asia trough. Thus, it can be observed that, among many external reasons for the extreme haze in 2014, only the pre-autumn Pacific SSTA was distributed similarly in 2013. The

240   EA/WR Rossby wave train was the prominent circulation contributing to WHD$_{NCP}$ in 2013, with a source located over the central-north Atlantic. We speculate that the air-sea interaction over north Atlantic excited the EA/WR pattern in the atmosphere and influenced WHD$_{NCP}$ remotely. The correlation coefficients between the EA/WR index and the pre-autumn SST in Atlantic were calculated and were significantly positive to the south of Greenland (Figure S7b). When the SSTA to the south of Greenland was positive, responses similar to EA/WR that occurred in the atmosphere. The pre-autumn SSTA in

245   the Atlantic in 2013 was similar to that shown in Figure S7b and might have remotely impacted WHD$_{NCP}$ via the EA/WR pattern. It should be noted that the SSTA of the key region in the Atlantic was negative and had an adverse effect on WHD$_{NCP}$ in 2014.

From the point of facilitating a larger amount of WHD$_{NCP}$, the associated circulation and external forcing in 2013 was different from that in 2014 and slightly weaker synthetically to a certain extent. The climate conditions influenced haze

250   weather on the premise that pollutant emissions were high in the recent years. The Shangdianzi site is the only GAWS in North China and was chosen to reflect the natural or background situation of the atmosphere. The mean mass concentrations of PM$_{2.5}$ in winter from 2004 to 2014 are plotted in Figure 11. The concentration in winter 2013 was the highest and nearly twice that in 2010 and 2014. The reasons for the serious haze pollution in 2013 were more compositive and complicated. The influences of the highest concentrations of PM$_{2.5}$ associated with atmospheric anomalies and external forcing added up and

255   contributed to the severe haze pollution. Compared with 2013, the concentrations measured by the two methods both decreased dramatically in 2014, indicating that the climate conditions accounted for a greater proportion.

Although the reconstructed haze datasets showed good representativeness for the meteorological phenomena and environmental disasters, the data in 2013 and 2014 were more qualitative than quantitative. To avoid a continuity problem,

the haze data of these two years were processed using composite analysis instead of correlation analysis in this study. In the

260 three case studies, 2010 and 2014 exhibited approximately equal $PM_{2.5}$ concentrations of the background atmosphere, which

was close to the mean value, but the concentration in 2013 was almost twice as large. Compared with 2013, the climate

conditions accounted for a greater proportion among the reasons for haze in 2010 and 2014. Even so, the associated

circulations and external forcings in 2010 were still slightly different from those in 2014. It is possible that not all of the

above factors might be found in a specific case study, i.e., only a few of these factors effectively led to the characteristics of

265 that case. The climate change influence on haze weather was based on the premise that the pollutant emission was high and

slowly changing in recent years, whose influence was removed simply by detrending. For peculiar cases with dramatically

changing atmospheric particles, such as 2013, the variation of pollution emission should be investigated. A brief summary of

the impacts of these factors on WHD_{NCP} is offered in Table 2.

Acknowledgements

270   This research was supported by the National Natural Science Foundation of China (Grants: 41421004 and 41210007) and

CAS-PKU Partnership Program.

References

Barnston A G, Livezey R E. 1987. Classification, seasonality and persistence of low frequency atmospheric circulation

patterns. Mon. Wea. Rev., 115: 1083–1126.

275 Chen H P, Wang H J. 2015. Haze days in North China and the associated atmospheric circulations based on daily visibility data

from 1960 to 2012. J. Geophys. Res. Atmos. 120(12): 5895–5909 DOI: 10.1002/2015JD023225.

Chen Y, Ebenstein A, Greenstone M, Li H. 2013. Evidence on the impact of sustained exposure to air pollution on life

expectancy from China's Huai River policy. Atmospheric Chemistry and Physics. 110: 12936–12941

China Meteorology Administration. 2014. The notification on the adjustment of haze phenomenon observing provisions and

280 revision of fog-haze observation data in 2013 by Observing and Forecasting Department Division. China Meteorology

Administration.

Cressman G. 1959. An operational objective analysis system, Mon. Wea. Rev. 87(10): 367–374.

Ding Y H, Liu Y J. 2014. Analysis of long-term variations of fog and haze in China in recent 50 years and their relations with atmospheric humidity. Sci. China Ser. D: Earth Sci. 57: 36–46 (in Chinese)..

285 Kalnay E, Kanamitsu M, Kistler R, Collins W, Deaven D, Gandin L, Iredell M, Saha S, White G, Woollen J, Zhu Y, Leetmaa A,Reynolds R, Chelliah M, Ebisuzaki W, Higgins W, Janowiak J,Mo KC, Ropelewski C, Wang J, Jenne R, Joseph D. 1996. The NCEP/NCAR 40-year reanalysis project. Bull. Am. Meteorol. Soc., 77: 437–471, doi: 10.1175/1520-0477(1996)077<0437: TNYRP>2.0.CO; 2.

Li Q, Zhang R H, Wang Y. 2015. Interannual variation of the winter-time fog–haze days across central and eastern China and
290 its relation with East Asian winter monsoon. Int. J. Climatol. 36 (1): 346–354, doi: 10.1002/joc.4350.

Liao X N, Zhang X, Wang Y, Liu W, Du J, Zhao L. 2014. Comparative analysis on meteorological condition for persistent haze cases in summer and winter in Beijing. Environ. Sci. Technol. 35(6): 2031–2044 (in Chinese).

Liu J P, Judith A. Curry, Wang H J. Mirong Song, Radley M. Horton. 2012. Impact of declining Arctic sea ice on winter snowfall. Proc. Natl. Acad. Sci., 109 (11): 4074–4079. DOI: 10.1073/pnas.1114910109

295 Liu Y Y, Wang L, Zhou W, Chen W. 2014. Three Eurasian teleconnection pattern: spatial structures, temporal variability, and associated climate anomalies. Clim Dyn. 42: 2817–2839

Rayner N A, Parker D E, Horton E B, Folland C K, Alexander L V, Rowell D P, Kent E C, Kaplan A. 2003. Global analyses of sea surface temperature, sea ice, and night marine air temperature since the late nineteenth century. J. Geophys. Res. 108 (14): 4407 doi: 10.1029/2002JD002670

300 Smith T, Reynolds R, Peterson T, Lawrimore J. 2008. Improvements to NOAA's historical merged land–ocean surface temperature analysis (1880–2006). J. Climat., 21: 2283–2296

Wallace J M, Gutzler D S. 1981. Teleconnection in the geopotential height field during the Northern Hemisphere winter. Mon. Wea. Rev., 109, 784–812, doi:10.1175/1520-0493(1981)109,0784:TITGHF.2.0.CO;2.

Wang D Q, Cui T, Si D, Shao X, Li Q Q, Sun C H. 2015. Features and Possible Causes for East Asian Winter Monsoon in
305 2014/2015. Meteorological Monthly. 41(7): 907–914(in Chinese).

Wang H J, Chen H P, Liu J P. 2015a. Arctic sea ice decline intensified haze pollution in eastern China, Atmos. Oceanic Sci. Lett., 8 (1): 1–9

Wang H J, He S P. 2015b. The North China/Northeastern Asia Severe Summer Drought in 2014. Journal of Climate. 28(17), 6667–668

310   Wang H J, Chen H P. 2016. Understanding the recent trend of haze pollution in eastern China: role of climate change, Atmos. Chem. Phys., 16: 4205–4211

Yao B, Vollmer M K, Zhou L X, Henne S, Reimann S, Li P C, Wenger A, Hill M. 2012. In-situ measurements of atmospheric hydrofluorocarbons (HFCs) and perfluorocarbons (PFCs) at the Shangdianzi regional background station, China, Atmos. Chem. Phys., 12, 10181–10193, doi:10.5194/acp-12-10181-2012, 2012.

315   Yin Y, Cheng J, Duan Y, Wei H, Ji R, Yu J, Yu H. 2011. Correlation analysis between the PM2.5, PM10 which were taken in the hazy day and the number of outpatient about breathing sections, breathing sections of pediatrics in Shanghai. Huan Jing Ke Xue 32(7): 1894–1898 (in Chinese).

Yin Z C, Wang H J, GUO W L. 2015a. Climatic change features of fog and haze in winter over North China and Huang-Huai Area. SCIENCE CHINA Earth Sciences, 58(8): 1370–1376.

320   Yin Z C, Wang H J, Yuan D M. 2015b. Interdecadal increase of haze in winter over North China and the Huang-huai area and the weakening of the East Asia winter monsoon. Chin. Sci. Bull. 60(15): 1395–1400 (in Chinese).

Yin Z C, Wang H J. 2015c. The relationship between the subtropical Western Pacific SST and haze over North-Central North China Plain. International Journal of Climatology, DOI: 10.1002/joc.4570

Zhang R H, Li Q, Zhang R N. 2014. Meteorological conditions for the persistent severe fog and haze event over eastern China

325   in January 2013. ScienceChina: Earth Sciences, 57: 26–35. doi: 10.1360/972013-150

Zhao N, Yin Z C, Wu F. 2014. Characteristics of persistent fog and haze process and its forming reason in Beijing. J. Meteorol. Environ. 30(5): 15–20 (in Chinese).

Zhao P S, Zhang X L, Xu X F, Zhao X J. 2011. Long-term visibility trends and characteristics in the region of Beijing, Tianjin, and Hebei, China. Atmospheric Research. 101(3): 711–718.

330   **Tables and Figures captions:**

Table 1. Correlation coefficients between WHD$_{NCP}$ and three teleconnection (EA/WR, WP and EU) indices. A single asterisk (*) indicates that the result exceeded the 95% confidence level, and double asterisks (**) indicate that it exceeded the 99% confidence level. Note: OS means 'original sequence', and 'detrended' means that the linear trend was removed.

Table 2. Summary of the various influnce factors for WHD$_{NCP}$. The "+++" indicates "more important"; "++" indicates

335   "important", "+" indicates "less important" , and blank indicates "not important".

Figure 1. Topographic map (shading; unit: m) of North China and the locations of 39 NCP observation sites (black circle). The NCP area is represented by a black rectangle, and the names of provinces and mountains are written in red and white, respectively.

Figure 2. Visibility of Beijing (green) and atmospheric compositions at BaoLian (blue) and Shangdianzi (red) stations at

340   02:00, 08:00, 14:00 and 20:00 LT from 1st Dec 2014 to 28th Feb 2015. The eight compositions included here are SO_2, NO, NO_2, NO_x, CO, O_3, $PM_{2.5}$ and NEP from top to bottom. The correlation coefficient was recorded as "CC", and the "N" denotes the number of composition samples. The total number of visibility observations was 360, which was adjusted to match the "N" of each composition after quality control and to compute CC.

Figure 3. Variation of WHD$_{NCP}$ from 1979–2014 (Units: days), the error bar represents one standard error among the

345   measured sites. For 2013–2014, the thresholds of 7.5 km (blue) and 10 km (gray) are both shown, and the dashed lines indicate the mean values for 1979–1992 and 1993-2012, respectively.

Figure 4. Distributions of WHD from 1979 to 2012 (a) and anomalies in 2014 relative to 1979-2012 (b).

Figure 5. Correlation coefficients between WHD$_{NCP}$ and circulations from 1979 to 2012 with linear trend was removed (a, c), and circulation anomalies in 2014 (b, d). The circulations in (a, b) are TS (shade) and SLP (contour) and those in (c, d) are

350   surface wind speed (shade) and wind vector (arrow).

Figure 6. Correlation coefficients between WHD$_{NCP}$ and winter H500 (a) / UV850 (b) from 1979 to 2012. The linear trend was removed, and shade indicates that CC exceeds the 95% confidence level. UV850 (arrow) and speed (shade) anomalies in winter 2014 (c) and 2010 (d). A and C represent anti-cyclone and cyclone, respectively.

Figure 7. Heterogeneous correlation map of the first SVD model for detrended and normalized (a) H500 during DJF and (b)

355 ASI during SON 1979–2014; (c) ASI anomaly during SON 2014. A and C represent anti-cyclone and cyclone, respectively.

Figure 8. Heterogeneous correlation map of the first SVD model for detrended and normalized (a) H500 during DJF and (b)

TS during DJF 1979–2014; (c) TS anomaly during DJF 2014. A and C represent anti-cyclone and cyclone, respectively.

Figure 9. Heterogeneous correlation map of the first SVD model for detrended and normalized (a) H500 during DJF and (b)

SST during ON 1979–2014; (c) SST anomaly during ON 2014. A and C represent anti-cyclone and cyclone, respectively.

360 **Figure 10.** Heterogeneous correlation map of the second SVD model for detrended and normalized (a) H500 during DJF and

(b) TS during SON 1979–2014; (c) TS anomaly during SON 2014. A and C represent anti-cyclone and cyclone, respectively.

Figure 11. Mean mass concentration of $PM_{2.5}$ in winter at Shangdianzi Station from 2004 to 2014 as measured by the TOEM

(solid) and β-ray (dash) method. The error bar represents one standard error among the different measured hours.

365

370

375

Table 1. Correlation coefficients between WHD$_{NCP}$ and three teleconnection (EA/WR, WP and EU) indices. A single asterisk (*) indicates that the result exceeded the 95% confidence level, and double asterisks (**) indicate that it exceeded the 99% confidence level. Note: OS means 'original sequence', and 'detrended' means that the linear trend was removed.

Pattern	OS	Detrended
EA/WR	0.36*	0.43**
WP	−0.06	0.41*
EU	0.34*	−0.13

380

Table 2. Summary of the various influnce factors for WHD$_{NCP}$. The "+++" indicates "more important"; "++" indicates "important", "+" indicates "less important" , and blank indicates "not important".

Factors	2010	2013	2014
EA/WR	++	++	++
WP	++		++
EU			++
PM$_{2.5}$ concentration	++	+++	++
Pre-autumn ASI	++		++
Winter TS	++		++
ON Pacific SSTA	+	++	++
Pre-autumn TS	++		++
SON Atlantic SSTA		++	

385
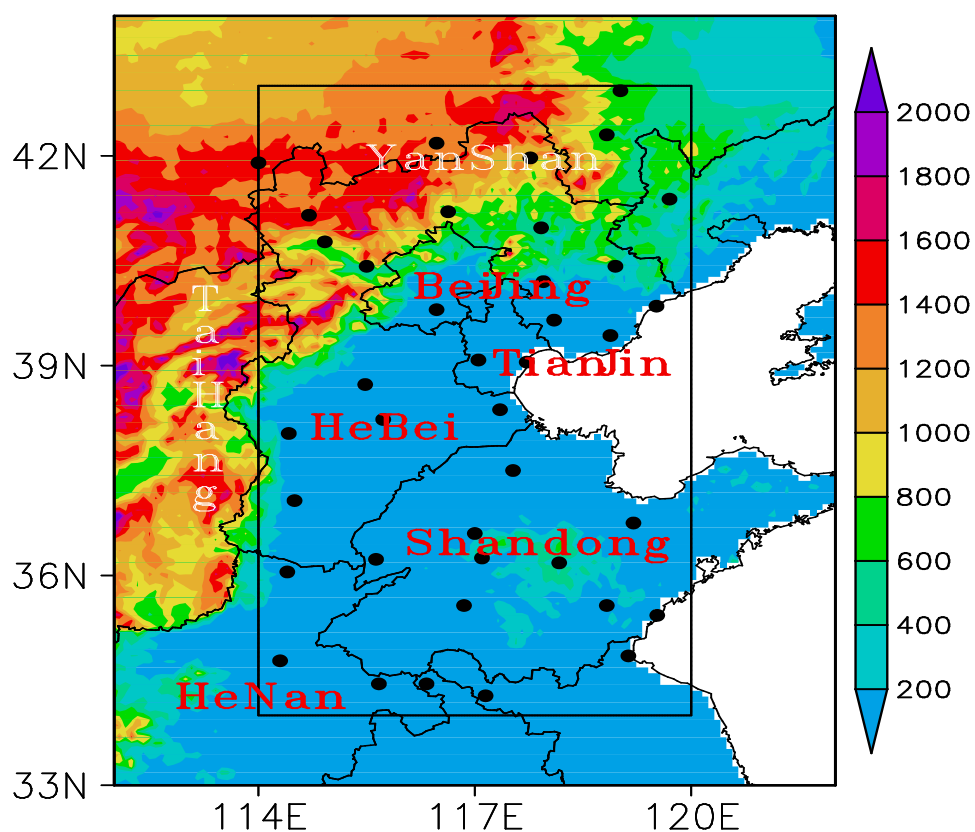
Figure 1. Topographic map (shading; unit: m) of North China and the locations of 39 NCP observation sites (black circle). The

390   **NCP area is represented by a black rectangle, and the names of provinces and mountains are written in red and white, respectively.**
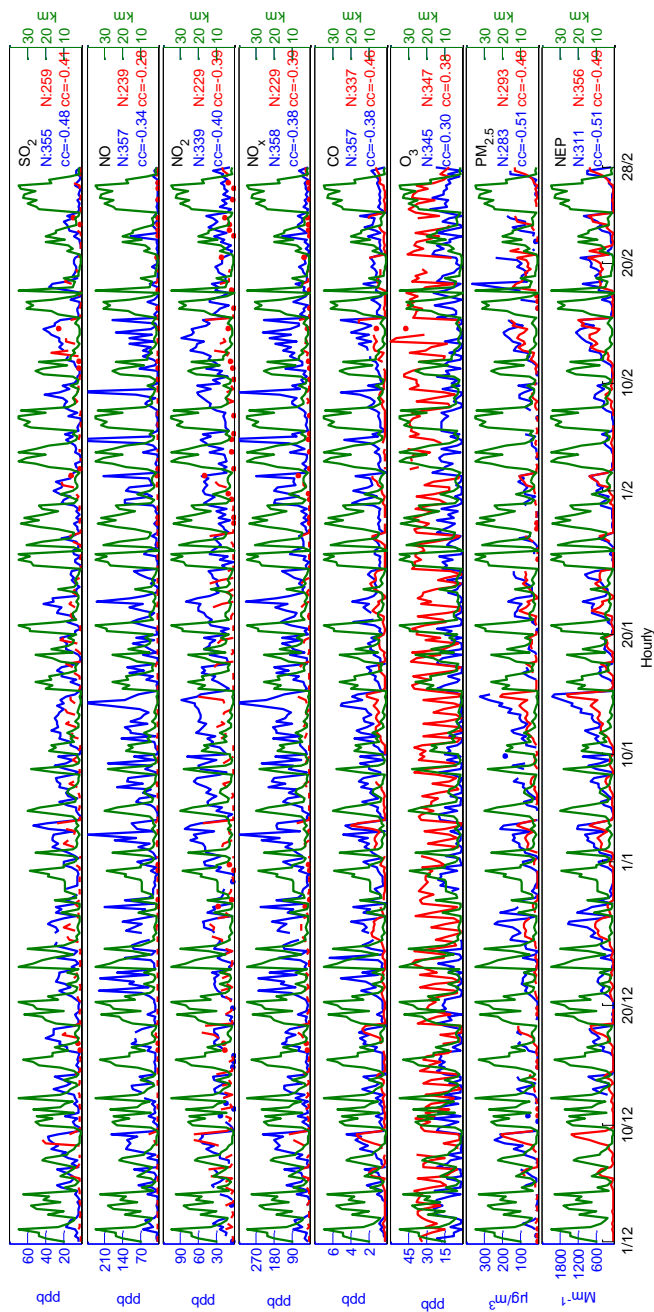
395 **Figure 2.** **Visibility of Beijing (green) and atmospheric compositions at BaoLian (blue) and Shangdianzi (red) stations at 02:00, 08:00, 14:00 and 20:00 LT from 1st Dec 2014 to 28th Feb 2015. The eight compositions included here are SO$_2$, NO, NO$_2$, NO$_x$, CO, O$_3$, PM$_{2.5}$ and NEP from top to bottom. The correlation coefficient was recorded as "CC", and the "N" denotes the number of composition samples. The total number of visibility observations was 360, which was adjusted to match the "N" of each composition after quality control and to compute CC.**
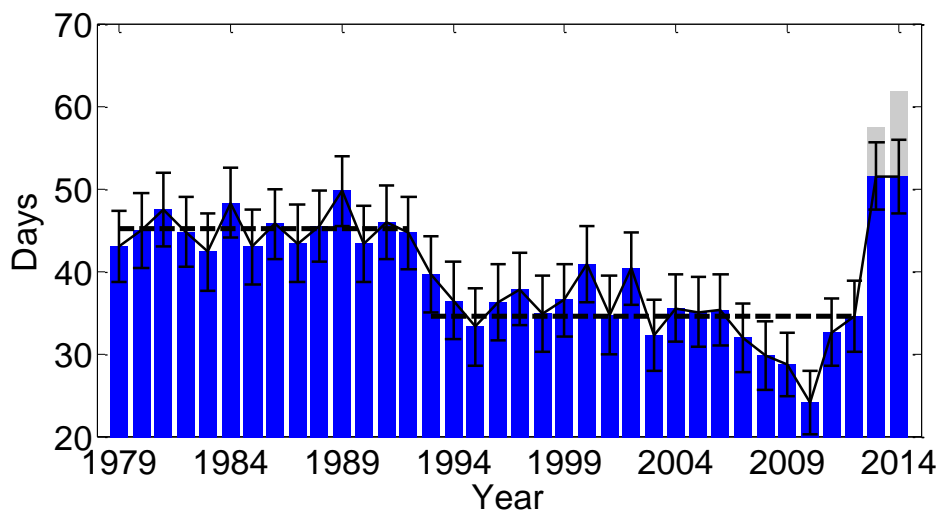
400

Figure 3. Variation of WHD$_{NCP}$ from 1979–2014 (Units: days), the error bar represents one standard error among the measured sites. For 2013–2014, the thresholds of 7.5 km (blue) and 10 km (gray) are both shown, and the dashed lines indicate the mean values for 1979–1992 and 1993-2012, respectively.

405
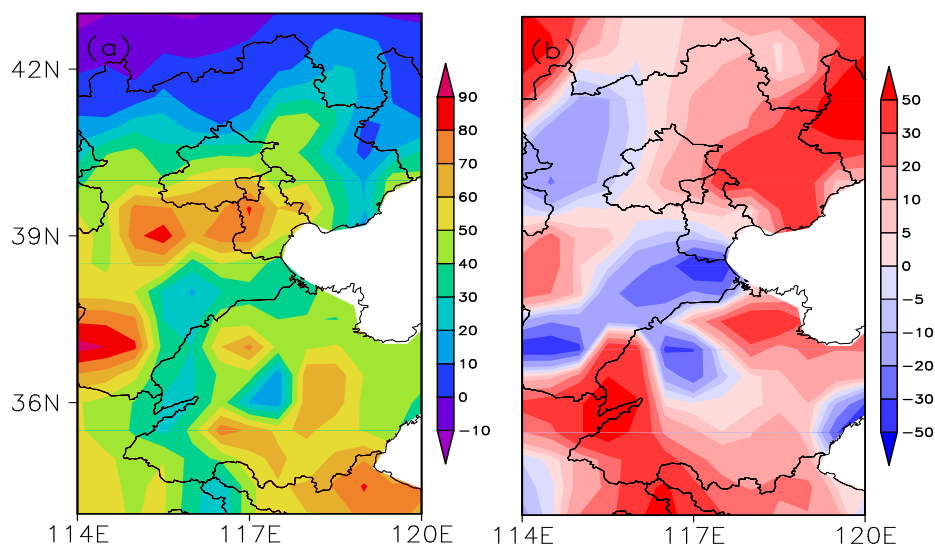
Figure 4. Distributions of WHD from 1979 to 2012 (a) and anomalies in 2014 relative to 1979-2012 (b).

410
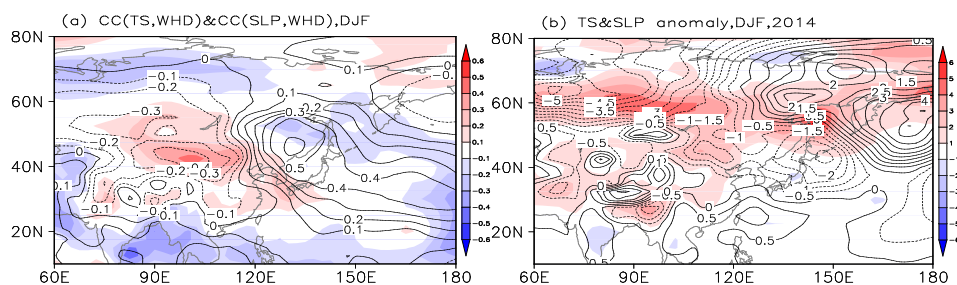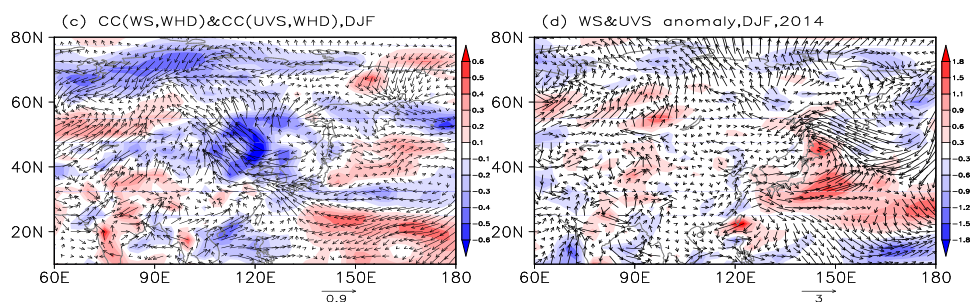
Figure 5. Correlation coefficients between WHD$_{NCP}$ and circulations from 1979 to 2012 with linear trend was removed (a, c), and circulation anomalies in 2014 (b, d). The circulations in (a, b) are TS (shade) and SLP (contour) and those in (c, d) are surface wind speed (shade) and wind vector (arrow).
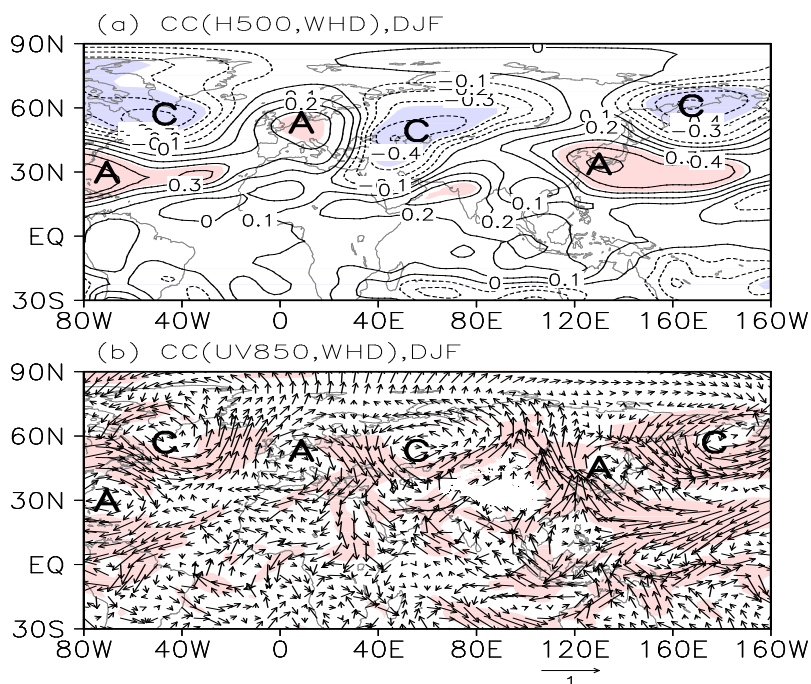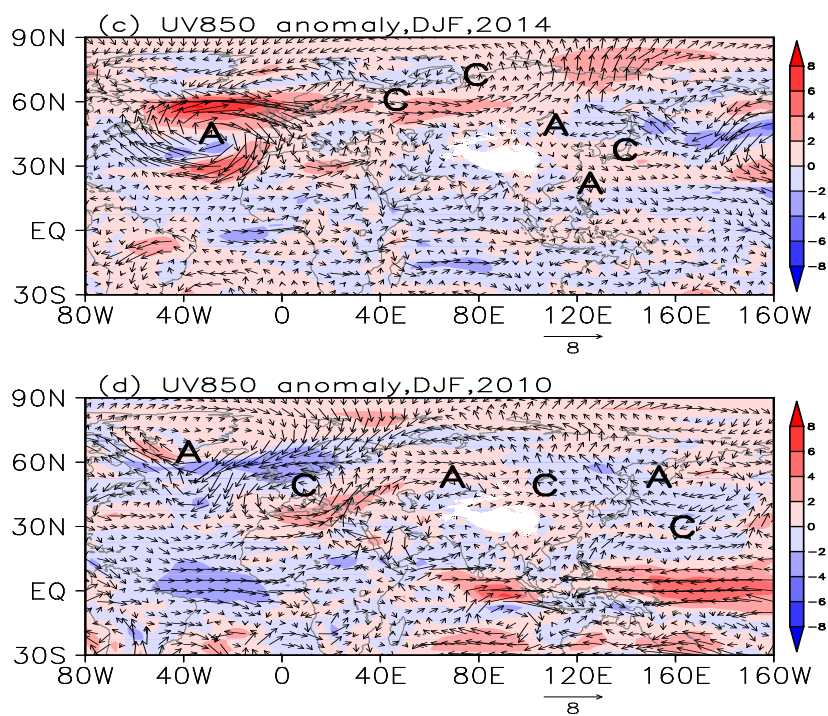
425

Figure 6. Correlation coefficients between WHD$_{NCP}$ and winter H500 (a) / UV850 (b) from 1979 to 2012. The linear trend was removed, and shade indicates that CC exceeds the 95% confidence level. UV850 (arrow) and speed (shade) anomalies in winter 2014 (c) and 2010 (d). A and C represent anti-cyclone and cyclone, respectively.

430
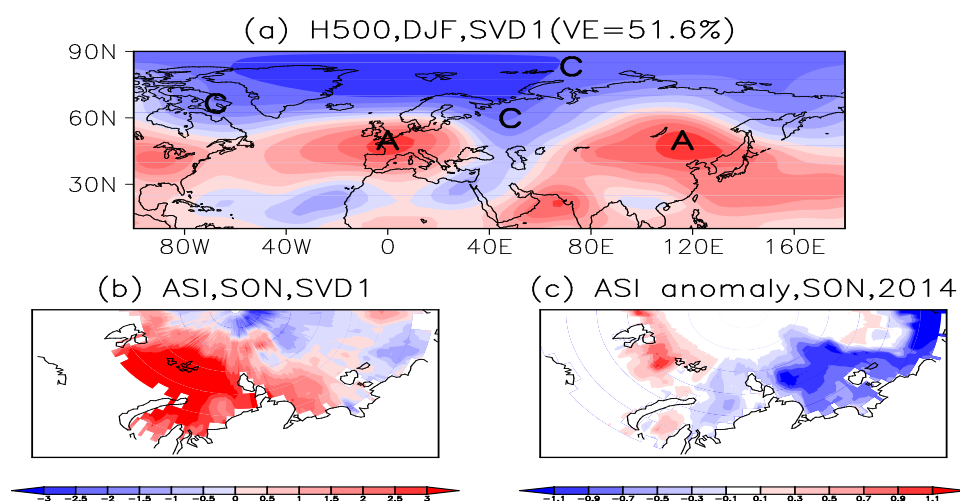
Figure 7. Heterogeneous correlation map of the first SVD model for detrended and normalized (a) H500 during DJF and (b) ASI during SON 1979–2014; (c) ASI anomaly during SON 2014. A and C represent anti-cyclone and cyclone, respectively.

435
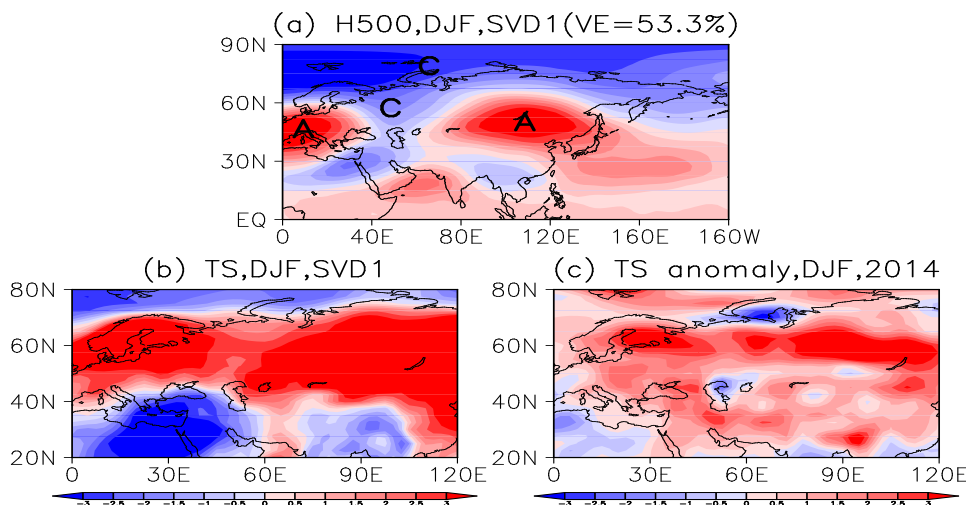
Figure 8. Heterogeneous correlation map of the first SVD model for detrended and normalized (a) H500 during DJF and (b) TS during DJF 1979–2014; (c) TS anomaly during DJF 2014. A and C represent anti-cyclone and cyclone, respectively.

440
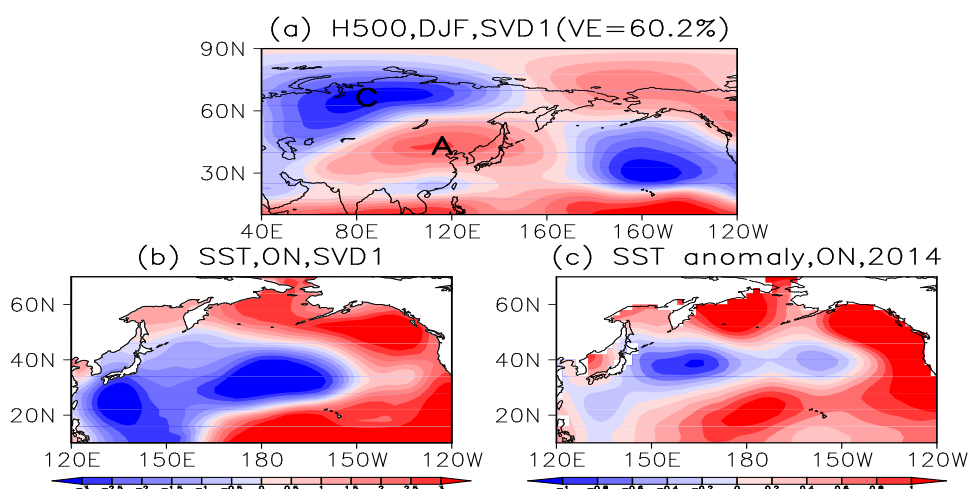
Figure 9. Heterogeneous correlation map of the first SVD model for detrended and normalized (a) H500 during DJF and (b) SST during ON 1979–2014; (c) SST anomaly during ON 2014. A and C represent anti-cyclone and cyclone, respectively.

450

455
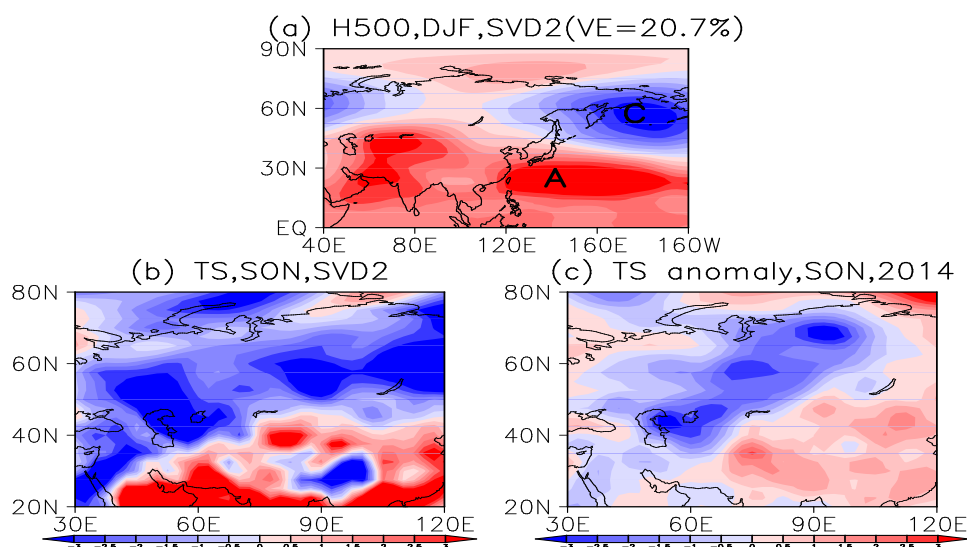
Figure 10. Heterogeneous correlation map of the second SVD model for detrended and normalized (a) H500 during DJF and (b) TS during SON 1979–2014; (c) TS anomaly during SON 2014. A and C represent anti-cyclone and cyclone, respectively.

460

465

Figure 11. Mean mass concentration of PM$_{2.5}$ in winter at Shangdianzi Station from 2004 to 2014 as measured by the TOEM (solid) and β-ray (dash) method. The error bar represents one standard error among the different measured hours.

470